# CALIBRATING COEFFICIENTS FOR PREDICTION OF DEPTH AVERAGED VELOCITY DISTRIBUTION

J.R. Khuntia[1] K. Devi[2] K.K. Khatua[3]

[1&2]*Research Scholar,Civil Engineering Department, National Institute of Technology,Rourkela,769008,India*

[3]*Associate Professor,Civil Engineering Department,National Institute of Technology,Rourkela,769008,India*

[1]*Email: jnanaranjan444@gmail.com,* [2]*Email: kamalinidevi1@gmail.com,* [3]*Email: kkkhatua@yahoo.com*

## ABSTRACT

The Shiono Knight method offers an improved numerical solution to predict depth averaged velocity distribution and boundary shear distribution in an open channel flow. While applying this method one has to calibrate the coefficients like $f$, $\lambda$ and $k$ which account for bed shear, lateral shear and secondary flow respectively. Experimental investigations have been carried out to find out the calibrating coefficients. These calibrating coefficients are found to vary laterally, flow depth to flow depth and due to change of the bed roughness. Experiments have been conducted on both trapezoidal and rectangular open channel for different flow conditions and roughness conditions. Keeping the geometry and flow conditions same, boundary roughness has been changed. The effect of roughness on evaluating the calibrating coefficients has been studied and modelled. Multi-linear regression models to predict $f$, $\lambda$ and $k$ have been attempted. Each model incorporates four non dimensional geometric, hydraulic and roughness parameters. The parameters are roughness ratio, relative lateral distance, aspect ratio Reynolds no. The paper demonstrates the ability of the model to provide depth averaged velocity distribution successfully for both smooth and rough channels under different flow condition recorded for this purpose as well as for FCF data for a better comparison.

***Keywords:*** *Shiono and Knight Method, calibrating coefficients, multi-linear regression, depth averaged velocity*

## 1. INTRODUCTION:

Several 1-D and 2-D approaches are presented by different researchers in this field however 2-D approach is more challenging. Tominaga et al. (1989) studied the velocity vectors and observed that the secondary currents flow toward the side wall along a horizontal plane that was located approximately at 0.6*H* (*H*=depth of flow). Wilkerson and McGahan (2005) developed and evaluated two models for predicting depth-averaged velocity distributions in straight trapezoidal channels. An analytical technique for finding the depth average velocity in an open channel has been presented by Maghrebi and Ball (2006). They compared their result applied to the river Severn with the best analytical results obtained by the depth-averaged Navier–Stokes equations. Tang & Knight (2008) presented two-dimensional analytical solution and compared with the conventional solution for three simple channel shapes and one trapezoidal compound channel. Yang (2010) investigated the influence of flow geometry on the depth-average shear stress and velocity in an open channel flow. They established a theoretical relationship between the boundary shear stress and depth-averaged apparent shear stress.

In a 2D approach, the momentum equation is simplified and the most commonly used is the Shiono & Knight (1990) approach (SKM model) as used in the CES (Conveyance Estimating System, UK). This method has been derived on depth averaging of the Navier-Stokes equations. The complexity of two-dimensional SKM model is to calibrate the three governing parameters (bed friction *f*, eddy viscosity coefficient $\lambda$ or turbulent friction and secondary flows $\Gamma$) before it can be applied successively to predict the depth averaged velocity in an open channel flow. According to Knight (1999) dimensionless eddy viscosity are in the range of 0.07–0.50, with ‘‘standard’’ values are taken from their experiment. They found that the calibration of their depth-averaged finite-element model was insensitive to the dimensionless eddy viscosity values. For evaluating the secondary flow parameters, the observations are taken from experimental of field observation results only. Though SKM is used in flow computation considering the 2-D flow effects, but the calibration coefficients of the model depend on the experimental and field observations only. Looking to the matter in view,

an attempt has been made to solve the SKM through suitable MATLAB programming and applying that to UK Flood Channel Facility (UK-FCF) and experimental channels at NITR.

## 2. EXPERIMENTAL SETUP AND PROCEDURES

In order to calibrate the analytical model of Shiono and Knight Model (SKM), two sets of data from NIT, Rourkela and FCF-UK were selected. First and second series of data sets selected from NIT, Rourkela for this analysis. For the first series of data, the cross section of main channel in rectangular channel with bottom (*2b*) dimension of 0.34m, height (*h*) of 0.113m over a length of 14m. The channel has a rigid bed surfaces by using the Perspex sheets of 6 to 10mm thick and having Manning's roughness value *n*=0.01.The flume was given a longitudinal slope of 0.003 so that water could flow inside channels under gravity. For the second series of data, experiments were carried out in the channel cross section of trapezoidal shape with bottom width (*2b*) dimension of 0.33m, height (*h*) of 0.11m and side slope 1:1 (*H:V*) over a length of 12m with longitudinal bottom slope of 0.0013. The Manning's roughness value *n* = 0.011. The discharges were measured by notch provided at entrance after water supplied to the channel by inlet pipe at upstream side. The third series of data chosen for the present analysis are from a large scale compound channel facility i.e. the UK Flood Channel Facility, located at the laboratories of HR Wallingford Ltd. shown in Figure 3. The details of geometrical and hydraulic parameters such as width of channel, aspect ratio, longitudinal slope of the channel etc. are summarized in Table 1. The experimental channels of NIT, Rourkela are shown in figure 1 and dimensions of experimental channels are shown in Figure 2. Figure 3 and Figure 4 are presented the general view of FCF channel and dimensions of FCF channels respectively. The model was developed and results were compared after the experiments were completed in both trapezoidal and rectangular channels.


**Figure 1.** Photo of fabricated experimental channels, NITR (a) Trapezoidal (b) Rectangular

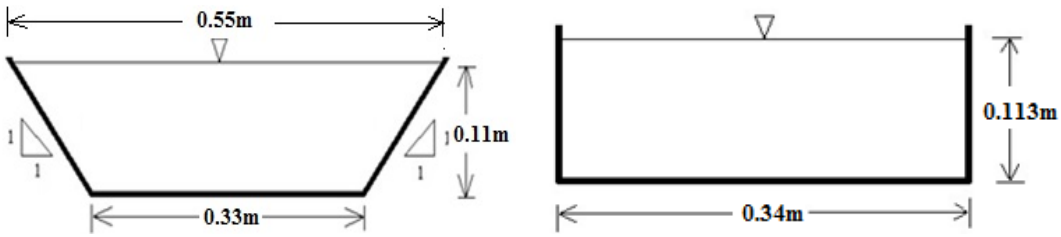


**Figure 2.** Dimensions of Experimental Channels, NITR (a) Rectangular (b) Trapezoidal

**Figure 3.** General view of the Flood Channel Facility (FCF) at H.R. Wallingford (Knight and Shiono 1990)

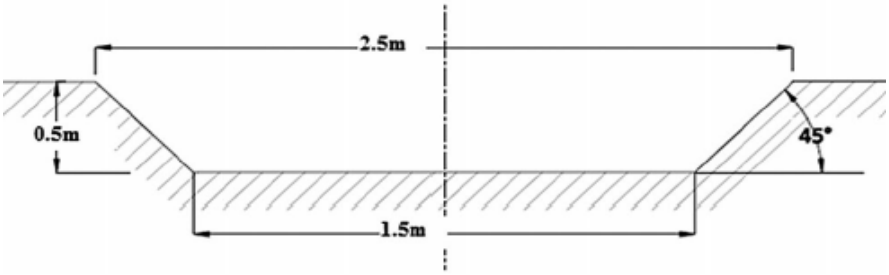


**Figure 4.** Dimension of FCF Channel

**Table 1.** The geometry and hydraulic data of the experimental channels

| Series | Width of channel *2b* (m) | Side wall angle | Flow depth *H* (m) | Manning's *n* | Discharge (*Q*) $m^3/s$ | Bed slope $S_0$ | Re |
|---|---|---|---|---|---|---|---|
| NITR_S1 | 0.33 | 45 | 0.08 | 0.011 | 0.0158 | 0.0013 | 28331 |
| | 0.33 | 45 | 0.09 | 0.011 | 0.016 | 0.0013 | 27238 |
| | 0.33 | 45 | 0.1 | 0.011 | 0.0241 | 0.0013 | 39156 |
| | 0.33 | 45 | 0.11 | 0.011 | 0.0256 | 0.0013 | 39770 |
| NITR_S2 | 0.34 | 90 | 0.076 | 0.01 | 0.0117 | 0.003 | 21349 |
| | 0.34 | 90 | 0.083 | 0.01 | 0.0143 | 0.003 | 25221 |
| | 0.34 | 90 | 0.09 | 0.01 | 0.016 | 0.003 | 27247 |
| | 0.34 | 90 | 0.099 | 0.01 | 0.0178 | 0.003 | 29065 |
| | 0.34 | 90 | 0.107 | 0.01 | 0.0201 | 0.003 | 31647 |
| FCF series | 1.5 | 45 | 0.149 | 0.009851 | 0.2023 | 0.00103 | 369000 |
| | 1.5 | 45 | 0.101 | 0.010078 | 0.1035 | 0.00103 | 201000 |
| | 1.5 | 45 | 0.049 | 0.010361 | 0.0299 | 0.00103 | 63200 |
| | 1.5 | 45 | 0.076 | 0.010067 | 0.064 | 0.00103 | 129000 |

## 3. THEORETICAL ANALYSIS OF SHIONO AND KNIGHT METHOD (SKM)

The Reynolds-averaged Navier–Stokes equations (or RANS equations) are time-averaged (Reynolds 1894) equations of motion. For steady uniform flows, the Reynolds-Average Navier-stokes equation (RANS) is simplified (Shiono and Knight 1988, Shiono and Knight 1991, Omran 2005, Tang and Knight 2008 and Sharifi 2009) as

$$\nu\frac{\partial^2\bar{u}}{\partial y^2}+\nu\frac{\partial^2\bar{u}}{\partial z^2}-\frac{\partial\overline{u'v'}}{\partial y}-\frac{\partial\overline{u'w'}}{\partial z}+g\left\{\frac{\partial h}{\partial x}-S_0\right\}=\frac{\partial\bar{u}\bar{v}}{\partial y}+\frac{\partial\bar{u}\bar{w}}{\partial z} \quad (1)$$

This generalized equation is applicable for obtaining the turbulent flow structure in different flow conditions. The RANS equation in x direction (longitudinal flow direction) can be simplified as

$$\rho\left[\frac{\partial\bar{u}\bar{v}}{\partial y}+\frac{\partial\bar{u}\bar{w}}{\partial z}\right]=\rho gS_0+\frac{\partial}{\partial y}\left(-\rho\overline{u'v'}\right)+\frac{\partial}{\partial z}\left(-\rho\overline{u'w'}\right) \quad (2)$$

The simplification of (2) has been done in SKM method. In equation (2) the first term is the secondary flow term consisting of lateral and vertical components of the velocity. The second term represents the weight component of water. The third and fourth term accounts for the apparent shear or Reynolds shear stresses in vertical and horizontal planes respectively. Considering the mean velocity component in z direction is negligible then $\bar{w}$ is equal to zero and $\tau_{yx}=-\rho\overline{u'v'}$, $\tau_{zx}=-\rho\overline{u'w'}$ and Integrating (2) over the total flow depth *H* we have.

$$\int_0^H\rho\left[\frac{\partial\bar{u}\bar{v}}{\partial y}+\frac{\partial\bar{u}\bar{w}}{\partial z}\right]dz=\rho\frac{\partial H(\bar{u}\bar{v})_d}{\partial y}\text{ and }\int_0^H\rho gS_0dz=H\rho gS_0 \quad (3)$$

Finally equation (3) is simplified to

$$\rho\frac{\partial H(\bar{u}\bar{v})_d}{\partial y}=\rho HgS_0+\frac{\partial}{\partial y}\left(\rho\lambda H^2\left(\frac{f}{8}\right)^{\frac{1}{2}}U_d\frac{\partial U_d}{\partial y}\right)-\frac{f}{8}\rho{U_d}^2\sqrt{1+\frac{1}{s^2}} \quad (4)$$

This is the simplified form of SKM. Here the 1st term in the left hand side is due to secondary current ($\Gamma$). The first term in the right hand side is gravitational term for a uniform flow, the second term is the Reynolds shear stress and the third term which is present is the bed shear. Therefore we can now state that equation (4) is dependent upon three calibration co-efficient $f$, $\lambda$, and $\Gamma$, which are related to local bed friction, eddy viscosity and the secondary flow respectively. Out of this three calibrating coefficients $f$, $\lambda$ are generally taken to be constant for a given channel which has been described later. Shiono & Knight (1990 &1991), Tominaga et al. (1989) and Tominaga & Nezu (1991) have investigated the secondary current flow in channels. Shiono and Knight (1991) proposed an analytical solution by taking suitable values from their own experimental results and concluded that the depth averaged velocity varies linearly in lateral direction therefore they replaced the left hand side term in the equation by a constant, $\Gamma$.

$$\frac{\partial}{\partial y}[H(\rho\bar{u}\bar{v})_d] = \Gamma \quad (5)$$

Putting the values from equation (5), the general solution for depth averaged velocity for constant flow depth region and variable flow depth domain can now be extracted from equation (4) as indicated in equation 6

$$U_d(y) = [A_1 e^{\gamma y} + A_2 e^{-\gamma y} + k']^{1/2} \quad (6)$$

### 3.1 Calibrating Coefficients

The three calibrating coefficients are $f$, $\lambda$,$\Gamma$ are defined as follows:

- ***Darcy-Weisbach friction factor (f)***

$$f = \frac{8gn^2}{R^{1/3}} \text{ (Global Friction factor)} \quad (7)$$

Also calculated by using following equation:

$$f = \frac{8\tau_b}{\rho {U_d}^2} \text{ (Locall Friction factor)} \quad (8)$$

- ***Eddy Viscosity Coefficient (λ)***

Turbulent flow is the flow in which random motion of smaller or larger masses of the fluid is superimposed upon some simple pattern of flow. So in a flow the molecular viscosity with respect to turbulence is called eddy viscosity. Dimensionless eddy viscosity coefficient, $\lambda$ depends on local shear velocity or average boundary shear velocity and flow depth $H$.

Then $\lambda$ is calculated by using the following equations:

$$\tau_b = \left(\frac{f}{8}\right)\rho {U_d}^2 \quad (9)$$

$$\bar{\tau}_{yx} = \rho\, \bar{\epsilon}_{yx} \frac{\partial U_d}{\partial y} \quad (10)$$

$$\bar{\epsilon}_{yx} = \lambda U_* H \quad (11)$$

$$\lambda = \frac{\bar{\epsilon}_{yx}}{U_* H} \quad (12)$$

- ***Secondary flow parameter (Γ)***

Secondary flow parameter $\Gamma$ is defined by the equation:

$$\Gamma = \frac{\partial}{\partial y}[H(\rho UV)_d] \quad (13)$$

- ***Secondary flow coefficients***

Secondary flow coefficients ($k_1$ *and* $k_2$) were evaluated from experimental data and then calibrated. Secondary flow coefficients and eddy viscosity of experimental channels with flow aspect ratio are tabulated in table 1.

Devi et al. (2016) applied the boundary conditions for the present analyses are

1. $(U_d)_i = (U_d)_{i+1}$
2. $\left(\frac{\partial U_d}{\partial y}\right)_i = \left(\frac{\partial U_d}{\partial y}\right)_{i+1}$
3. $U_i = 0$

Applying the above boundary conditions to equation (6), a programming (using MATLAB) has been performed to find the depth average velocity form point to points laterally along the width of the channel. Secondary flow coefficients and eddy viscosity of experimental channels, NITR after calibration has been given in table 1.

**Table 1.** Secondary flow co-efficient and eddy viscosity of experimental channels, NITR

| Geometry Type | Roughness Type | Aspect Ratio (*2b/H*) | Secondary Flow Coefficients | | $\lambda$ |
|---|---|---|---|---|---|
| | | | Constant Flow domain ($k_1$) | Variable Flow domain ($k_2$) | |
| Rectangular | Smooth | 3.178-4.474 | 0.356-0.315 | - | 0.74755<br>-0.0577 |
| Trapezoidal | Smooth | 3.000-4.125 | 0.590-0.660 | 1.45-1.35 | -0.02211<br>-0.15541 |
| Trapezoidal | Rough(Type-1*) | 3.667-4.714 | 0.720-0.600 | 1.4-1.1 | 0.266497<br>-0.19146 |
| Trapezoidal | Rough(Type-2*) | 3.667-4.714 | 0.540-0.520 | 1.3-1.1 | 0.083642<br>0.433024 |

Type-1* small gravel of size 7 mm to 20 mm (*n*=0.02), Type-2* plastic mat of thickness 15mm (*n*=0.024)

## 4. RESULTS AND ANALYSIS

### 4.1 Friction factor variation

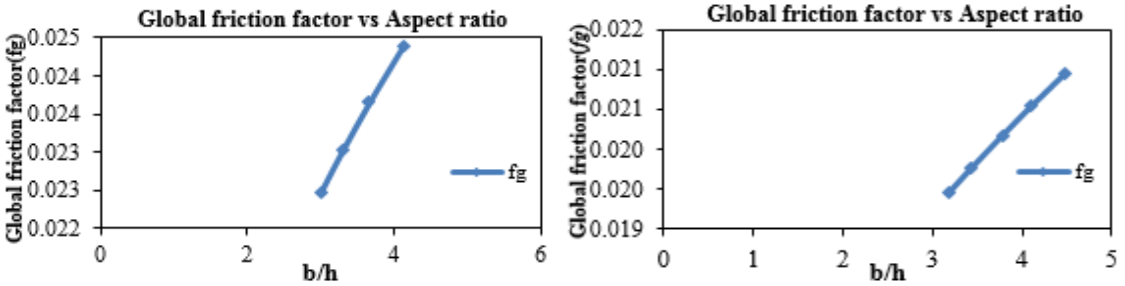


**Figure 2.** Variation of global friction factor for (a) Trapezoidal smooth channel, (b) Rectangular smooth channel, NITR

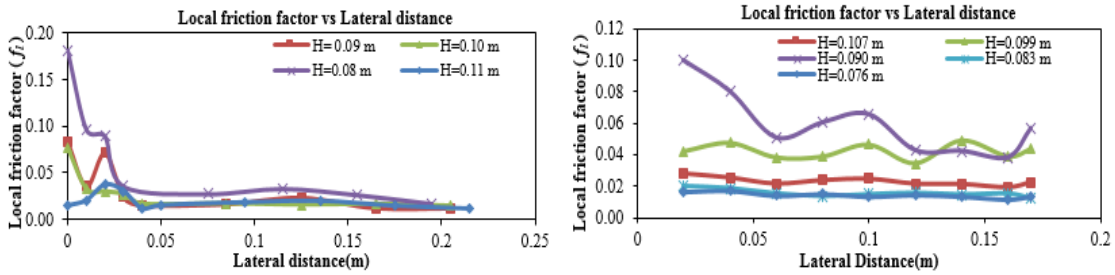


**Figure 3.** Variation of local friction factor for (a) Trapezoidal smooth channel (b) Rectangular smooth channel, NITR

- The global friction factors are of increasing in magnitude with aspect ratio in smooth trapezoidal and rectangular channel as shown in Figure 2.
- The variation of local friction factors for each flow depth is higher at side wall regions than bed regions in trapezoidal channel and it remains constant along the lateral cross section of rectangular channel as shown in Figure 3.

## 4.2 Eddy viscosity coefficient

In the mid-nineteenth century, some investigators were suggested "eddy viscosity" concept in turbulent flow which is an important factor to propose a general relationship of shear stress and shear strain, to relate the mean rate of deformation to the turbulent stresses (Schlichting, 1979, Davidson, 2004):

$$\tau_{xz}{}^{R} = \bar{\rho}\overline{u'w'} = \varepsilon_t\left(\frac{\partial u}{\partial x} + \frac{\partial w}{\partial z}\right) = (\mu_l + \mu_t)\left(\frac{\partial u}{\partial x} + \frac{\partial w}{\partial z}\right) \quad (16)$$

where the eddy viscosity $\varepsilon_t$ is the sum of the laminar viscosities ($\mu_l$) and turbulent viscosities ($\mu_t$). The eddy viscosity is observed as a coefficient of momentum transfer intimating the transfer of momentum from lower velocity to its higher and vice versa (Finnmore and Franizi, 2002).

The variation of eddy viscosity co-efficient due to formation of eddies in flow pattern with the lateral distance throughout the cross section of rectangular smooth channel have been given in Figure 4.

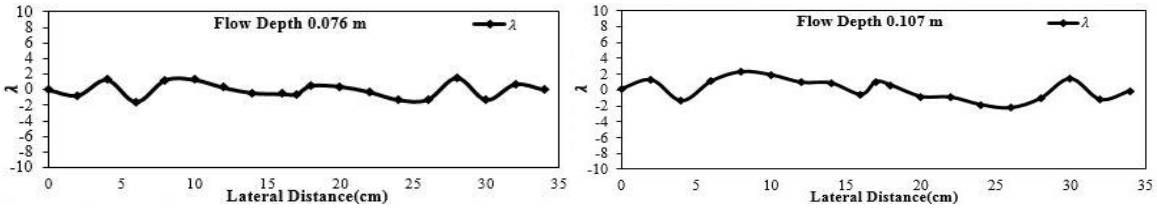


**Figure 4.** Eddy viscosity co-efficient in smooth rectangular channel

The variation of eddy viscosity co-efficient due to formation of eddies in flow pattern with the lateral distance throughout the cross section of trapezoidal smooth channel for different flow depths have been presented in Figure 5..

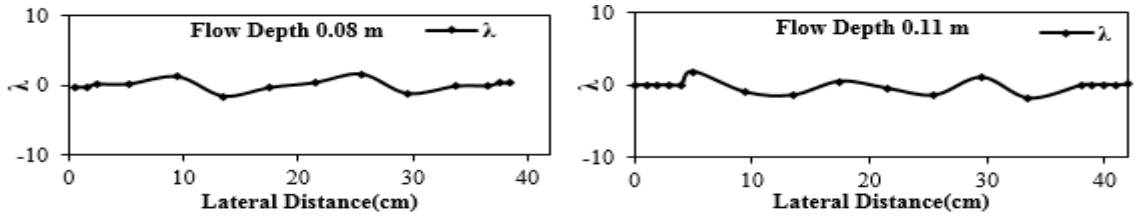


**Figure 5.** Variation of eddy viscosity co-efficient in smooth Trapezoidal channel

## 4.3 Secondary flow coefficients

After calibration the obtained value of secondary flow coefficient in constant flow domain $k_1$ and in variable flow domain $k_2$ with flow aspect ratio ($2b/h$) have been plotted in figure 6 and 7 respectively.

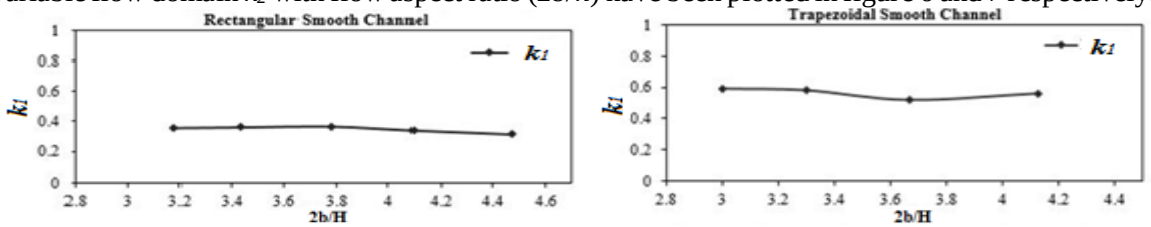


**Figure 6.** Variation of Secondary coefficient in constant flow domain $k_1$ with aspect ratio ($2b/H$)

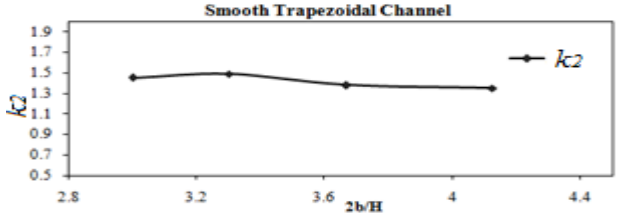


**Figure 7.** Variation of Secondary coefficient in variable flow $k_2$ with aspect ratio ($2b/H$)

### 4.4 Depth averaged velocity distribution

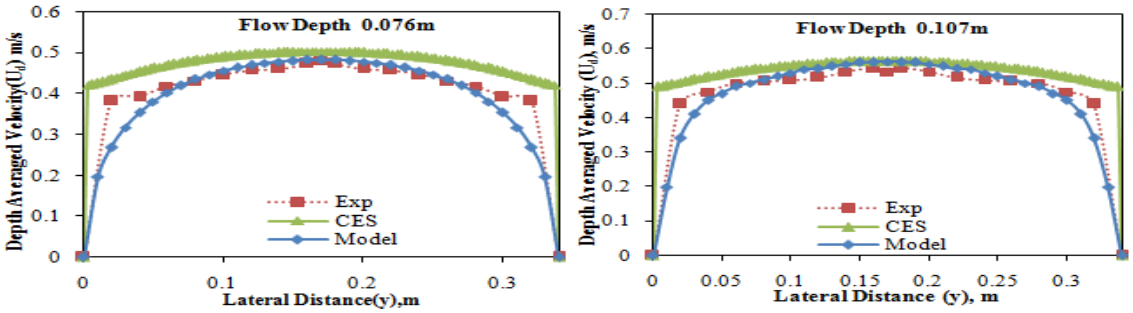


**Figure 8.** Depth averaged velocity of different flow depths for Smooth Rectangular Channel

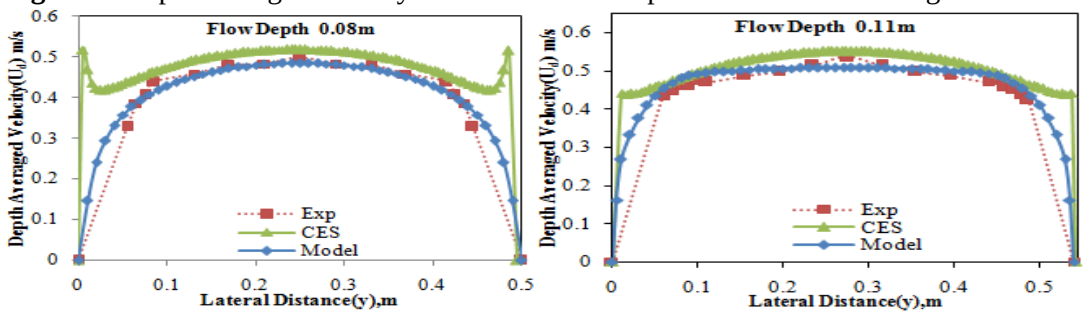


**Figure 9.** Depth averaged velocity of different flow depths for Trapezoidal smooth Channel

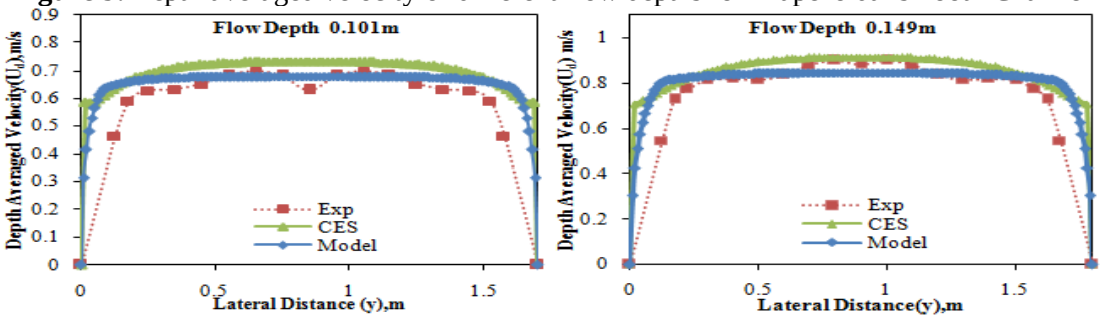


**Figure 10.** Depth averaged velocity of FCF Channel series for in-bank conditions

***Observations:***

Figure 8 represents the depth averaged velocity distribution for the present experimental smooth channel with rectangular geometry both the CES and Model has been applied to plot the depth averaged velocity distribution.

Similarly in Figure 9 shows the comparison of the CES result and the model with the experimental results for trapezoidal geometry. Here also model using the new calibrating coefficient values provides better results than CES.

The strength of the proposed approach has been applied to the FCF channels inbank flow conditions. Figure 10 shows the results for lower and higher flow depths. In both of the cases the present model using the new calibrating coefficient is providing better results than the SKM with constant values of calibrating coefficients.

These results indicate the proper calibrating coefficient values should be considered while modeling the depth averaged velocity using SKM in an open channel flow.

## 5. CONCLUSIONS

Experimental investigations have been performed for finding the calibrating coefficients of an open channel flow of different geometry (i.e., rectangular and trapezoidal) and flow conditions.

The global friction factors are of increasing in magnitude with aspect ratio in smooth trapezoidal and rectangular channel. The variation of local friction factors for each flow depth is higher at side wall regions than bed regions in trapezoidal channel and it remains constant along the lateral cross section of rectangular channel.

It can be observed that from given variation of eddy viscosity coefficient at the side wall region higher magnitude of $\lambda$ as compared to central region of channel where approximate constant values of $\lambda$ in smooth trapezoidal channel.

The model using the new calibrating coefficient values matches with experimental results better than the previously SKM model using the software CES for both rectangular and trapezoidal geometry.

The strength of the proposed approach has been applied to the FCF channels of inbank flow conditions which have been also provided better results than the CES, i.e., SKM with constant values of calibrating coefficients.

## REFERENCES

Davidson PA (2015) Turbulence: an introduction for scientists and engineers. Oxford University Press; 2015.
Devi K, Khatua KK, Das BS (2016) A numerical solution for depth-averaged velocity distribution in an open channel flow. ISH Journal of Hydraulic Engineering. 2016 May 22:1-10.
Finnemore JE, Franzini JB (2002) Fluid mechanics. McGraw-Hill; 2002.
Knight DW (1999) Flow mechanisms and sediment transport in compound channels. International Journal of Sediment and Research, 2:028.
Knight DW, Shiono K (1990) Turbulence measurements in a shear layer region of a compound channel. Journal of hydraulic research, 28(2):175-96.
Maghrebi MF, Ball JE (2006) New method for estimation of discharge. Journal of hydraulic Engineering, 132(10):1044-51.
Omran MN (2005) Modelling stage-discharge curves, velocity and boundary sheer stress distributions in natural and artificial channels using a depth-averaged approach. Doctoral dissertation, University of Birmingham, UK.
Reynolds O (1894) On the dynamical theory of incompressible viscous fluids and the determination of the criterion. Proceedings of the Royal Society of London. 1894 Jan 1;56(336-339):40-5.
Schlichting H (1979) Boundary-layer theory. McGraw Hill, NewYork, 459-465.
Sharifi S (2009) Application of evolutionary computation to open channel flow modelling. Doctoral dissertation, University of Birmingham, UK
Shiono K, Knight DW (1988) Two-dimensional analytical solution for a compound channel. In Proc., 3rd Int. Symp. on refined flow modeling and turbulence measurements, 503-510.
Shiono K, Knight DW (1990) Mathematical models of flow in two or multi stage straight channels. In Proc. Int. Conf. on River Flood Hydraulics, 229-238.
Shiono K, Knight DW (1991) Turbulent open-channel flows with variable depth across the channel. Journal of Fluid Mechanics, vol. 222, 617-646.
Tang X, Knight DW (2008) A general model of lateral depth-averaged velocity distributions for open channel flows. Advances in Water Resources, 31(5):846-857.
Tominaga A, Nezu I (1991) Turbulent structure in compound open-channel flows. Journal of Hydraulic Engineering, 117(1):21-41.
Tominaga A, Nezu I, Ezaki K, Nakagawa H (1989) Three-dimensional turbulent structure in straight open channel flows. Journal of hydraulic research, 27(1):149-173.
Wilkerson GV, McGahan JL (2005) Depth-averaged velocity distribution in straight trapezoidal channels. Journal of Hydraulic Engineering, 131(6):509-12.
Yang SQ (2010) Depth-averaged shear stress and velocity in open-channel flows. Journal of Hydraulic Engineering, 136(11):952-8.